J Mater Sci (2009) 44:1469–1476
DOI 10.1007/s10853-008-3037-8

Effect of polyurethane composition and the fabrication process on scaffold properties

Monika Bil · Joanna Ryszkowska · Krzysztof J. Kurzydłowski

Received: 31 January 2008 / Accepted: 7 October 2008 / Published online: 6 November 2008

Abstract The microdomain structure of polyurethanes (PUR) determines their unique physical properties and makes polyurethanes attractive candidates for various tissue engineering applications. 3D scaffolds based on polyurethanes with different contents of hard segments were fabricated by a salt-leaching/polymer coagulation method. The process parameters were carefully considered, particularly the polymer solution concentration and characteristics of the polyurethane, which are the critical parameters for the control of porosity and pore size distribution. In this study, 3D polyurethane scaffolds were fabricated with interconnected pores and porosity from 64% to 80%. Pore size distribution was evaluated using quantitative image analysis and mercury intrusion porosimetry (MIP). The scaffolds fabricated from polyurethanes with 70 wt.% of hard-domain content were found to have the best compression properties.

Introduction

Scaffold-based tissue engineering requires a temporary matrix for transplanted or host cells, which provides a specific environment and space for tissue development. Tissue regeneration through cell implantation in scaffolds depends mainly on the structure of the scaffold and the nature of the biomaterials [1]. The scaffold structure is characterized by the pore size and shape, the pore size distribution, the porosity, the interconnectivity and the pore throat size. Highly porous structures with an interconnected pore network facilitate cell proliferation and migration through the scaffold, ensure proper transport of nutrients and cell waste removal [2]. The effect of pores size on tissue ingrowths and an optimum pore size for different kinds of cells has been demonstrated in [3–5]. The macropores of the size in the range of 100–400 μm are considered optimal for bone tissue formation [6]. However, this size remains still a matter of controversy [7]. Macroporosity with pore size of 150–900 μm allows for nutrient supply and waste removal of cells grown on the scaffold. Micropores enhance cell attachment, ion exchange and bone-like apatite formation [8]. Although high porosity is very desirable from a biological point of view, it reduces the mechanical properties of the scaffold. Therefore, researchers seek a balance between total pore volume and mechanical strength, especially in scaffolds designed for load-bearing tissues, such as bone and cartilage.

A number of methods have been developed to fabricate polymer scaffolds [9]. One of the most common techniques for producing porous 3D scaffolds is the particulate-leaching method, which uses inorganic salt particles, paraffin and gelatin or ice [10–12]. The salt-leaching technique allows for control of the pore size and porosity by varying the size and amount of leachable particles. Unfortunately, this method can produce only thin wafers that lack interconnectivity between pores [13]. In order to overcome these disadvantages, the particulate-leaching technique has been combined with other methods, such as phase separation, emulsion freeze-drying, gas foaming, and compression moulding [14–16]. A number of polymer scaffolds are prepared by controlled phase separation of polymer solutions into two phases. The phase separation can be induced thermally or isothermally by mass transport and the exchange of solvent for non-solvent. In this method, a polymer solution is immersed in a non-solvent

M. Bil (✉) · J. Ryszkowska · K. J. Kurzydłowski
Warsaw University of Technology, Faculty of Materials Science and Engineering, Woloska 141, 02-507 Warsaw, Poland
e-mail: mbil@meil.pw.edu.pl

bath. When a good solvent in the polymer solution is exchanged for non-solvent, the polymer precipitates and a porous structure forms. Depending on precipitation conditions determined in part by the composition of the polymer solution, a non-solvent bath and polymer-type phase separation by nucleation and growth can be initiated for a liquid/liquid phase separation process, a crystallization process or a combination of both processes [17].

Polyurethanes (PUR) are attractive candidates for biomedical applications [18]. These polymers, contain hard and soft segments which allow for more subtle control of their structure and properties. The hard, rigid segments are produced by the reaction between the diisocyanate and the chain extender, whereas polyether, polyester, or polycarbonate diol comprises the soft segments. Hard domains act as reinforcing filler in the soft matrix. The hard-segment content influences the degree of phase separation, which in turn affects physical and mechanical properties [19–21], degradation rate and biocompatibility [22, 23]. By varying the molecular weight of polyol and the composition of the different segments, properties of PUR can be tuned up for use in many areas of tissue engineering, either for reconstruction of soft tissue or for cartilage and bone regeneration [24–28].

The objective of this study was to develop polyurethane porous scaffolds by salt leaching/polymer coagulation method. Polyurethanes with different contents of hard segments were synthesized. The effect of solution concentration on porosity and pore size distribution was evaluated in the context of optimum scaffold architecture and processing route.

Experimental

Materials

The following reactants were used in the synthesis of polyurethane: 4,4-methylenebis(cyclohexyl diisocyanate) (HMDI); Poly(ε-caprolactone) diols (PCL diol) with molecular weight ranging from 530 to 1250 Da; and dibutyltin dilaurate (DBTDL), purchased from Aldrich Chemical Co. (Germany). Ethylene glycol (EG) (POCH, Gliwice) was dried under molecular sieve. 1-methyl–2-pyrrolidone was supplied by Fluka, Germany. The other chemicals were used as received.

Polyurethane synthesis

Polyurethanes (PUR) were synthesized in bulk by a two-step polymerization method. A typical experimental procedure is outlined as follows. The PCL diol was dried under vacuum for 2 h at 120 °C. After cooling to 60 °C, HMDI and the catalyst were added to the melt and stirred under vacuum for 1 h at 60 °C. Next, EG was added and the reaction mixture was stirred in air atmosphere until it became clear. At the end, the reaction mixture was stirred under vacuum for additional 3 min, followed by curing at 110 °C for 8 h. This procedure, was used to synthesize PUR with different contents of hard segments. The physical properties of the PUR samples obtained are listed in Table 1.

Polyurethane foam preparation

Porous polyurethane structures were fabricated by the polymer coagulation combined with salt-particle leaching method. The PUR were ground at liquid nitrogen temperature with a laboratory grinder (Retsch ZM 200, Germany) and dissolved in 1-methyl-2-pyrrolidone at a concentration of 15 wt.% and 20 wt.%. The NaCl crystals were fractionated to the size ranging from 300–420 μm. The particles were subsequently incorporated into the polyurethane solution with mass ratio of polymer to NaCl, 1:5. The polymer/salt/solvent mixture was poured into a teflon mould (6 mm in diameter) and immersed in distilled water for 2 days, during which time precipitation of the polymer and leaching of the salt particles occurred simultaneously. Water was gently stirred and changed several times in order to increase salt leaching and solvent removal. The obtained porous polyurethane samples, of thickness approximately 6 mm, were dried under vacuum at 37 °C.

Methods

The molecular weight (M_w) and molecular weight distribution (MWD) of the polymers were determined by gel permeation chromatography (GPC) using a polystyrene standard for calibration. Measurements were made at 45 °C with DMF as a solvent.

Scaffold morphology was investigated via scanning electron microscopy (SEM) (HITACHI S-2600 N). Specimens were cut using a razor blade parallel to the surface. The resulting cross-sections were gold coated under vacuum using an automatic coating sputter which was set at 10 mA for 3 min (Polaron SC7640). Quantitative analysis of the pore sizes was carried out using Metilo computer software. In order to define pore geometry more precisely, the samples for quantitative analysis of the SEM images were infiltrated with paraffin under vacuum. After paraffin embedding, three random sections of the samples were cut by a microtome (Leica RM2165) at −10 °C. The resulting cross-sections were gold coated in the same manner as above. The SEM images were obtained using an accelerating voltage of 15 kV. A back-scattered electron-imaging mode (BSE) was applied for higher contrast between

Table 1 Chemical and physical properties of bulk polyurethanes (PUR)

PUR	PCL diol M_n	HMDI/PCL/EG Molar ratio	Hard segments content (wt.%)	M_w	MWD	Density (g/cm^3)	Young's Modulus (MPa)
PUR4PCL1250	1250	4:1:3	50	363800	2.73	1.1329	39
PUR2PCL530	530	2:1:1	52	374500	3.93	1.1478	38
PUR4PCL530	530	4:1:3	70	64995	2.45	1.1507	32

M_w average molecular weight, *MWD* molecular weight distribution

paraffin-filled pores and polymer matrix. The grey-scale images were filtered, the contrast adjusted, and a threshold applied to detect the dark regions of the sample. Additional manual correction of pore boundaries was performed. The frequency distribution of average Feret's diameter (D) throughout the matrix and volume fraction (Vv, %) of the pores was calculated [29].

Mercury intrusion porosimetry (Micromeritics Autopore II 9220) was used to determine pore size distribution and open porosity (P_o) of the foams. In this technique, mercury is intruded into pore spaces under high pressure. As mercury intrusion occurs, the cumulative volume of the intruded mercury at each pressure step is recorded in an intrusion curve. Using the Washburn equation, pore sizes and pore volume distribution by pore size are calculated [30].

Total porosity (P_t) of the scaffolds was calculated as follows:

$$P_t = (1 - q_{\text{scaffold}}/q_{\text{polymer}}) \times 100\% \quad (1)$$

where q_{scaffold}—the scaffold density determined by measuring the dimensions and the mass of the scaffold, q_{polymer}—the density of PUR (Table 1).

Compressive strength and compressive modulus were carried out on a MTS testing machine (model Q Test/10) with a 1 kN load cell. Compressive test was performed on cylindrical samples (6 mm in diameter and 4.2 mm thick) at a crosshead speed of 0.7 mm/min. The reported values are the average of five tests for each type of PUR scaffold. All these tests were carried out at an ambient temperature. The compressive modulus was evaluated from the linear elastic region of the stress–strain curve. The compression strength was determined at 10% compression.

Results and discussion

In this study, thermoplastic polyurethane 3D scaffolds with different contents of hard segments were fabricated for tissue engineering applications. The salt-leaching/polymer-coagulation technique was applied to produce a porous structure. As shown in the earlier studies [31, 32], the salt particle leaching/combined with phase separation results in the creation of a multi-porous structure. The larger pores typically result from the extraction of the porogen particles, whereas the smaller pores are characteristic of the combinatory method. The physical properties of the scaffolds obtained by this method are influenced by polymer solution concentration [5]. SEM observations of the foams revealed the presence of an interconnected porous network with three distinct pore morphologies (Figs. 1 and 2). The macropores were roughly cubic in shape and seemed to be homogeneously distributed in the polymer matrix (Fig. 1a–d). Only PUR_70_15 and PUR_70_20 presented markedly different morphologies, with thicker and highly porous walls between pores (Fig. 1e, f). The hard-segment content in the polyurethane matrix is much higher than in PUR_50 and PUR_52 scaffolds; the effect of this higher content on the immersion precipitation process can therefore be isolated. These observations are consistent with the finding of Lee et al. [33] who reported that PUR with a high concentration of the hard segment were likely to undergo liquid–liquid phase separation combined with crystallization.

In the SEM micrographs at higher magnification, the surface of the macropores are seen to be porous themselves (Fig. 2). Open cellular micropores with a maximum size of approximately 20 μm were observed. This morphology suggests that a spinodal decomposition mechanism was responsible for these structures, as similarly reported by Nam et al. [34]. Moreover, apart from micropore interconnections, all prepared foams directly connect through round pore throats. Improved interconnectivity was observed for scaffolds produced from 15 wt.% solution in comparison with scaffolds prepared from 20 wt.% (Fig. 1). The SEM observations allow to conclude that the obtained scaffolds present a broad size distribution of pores, which can be divided into three categories: macropores; pore throats, which connect the macropores; and micropores distributed on the walls of the macropores.

As evaluated by mercury intrusion porosimetry, the P_o of prepared scaffolds ranged from 64% to 80% depending on the polymer solution concentration and polyurethane type. The total porosity ranges from 66% to 81% (Table 2). No difference between open and total porosity was observed for PUR_50_15 and PUR_50_20 scaffolds. These results indicate that there is no closed cell porosity present

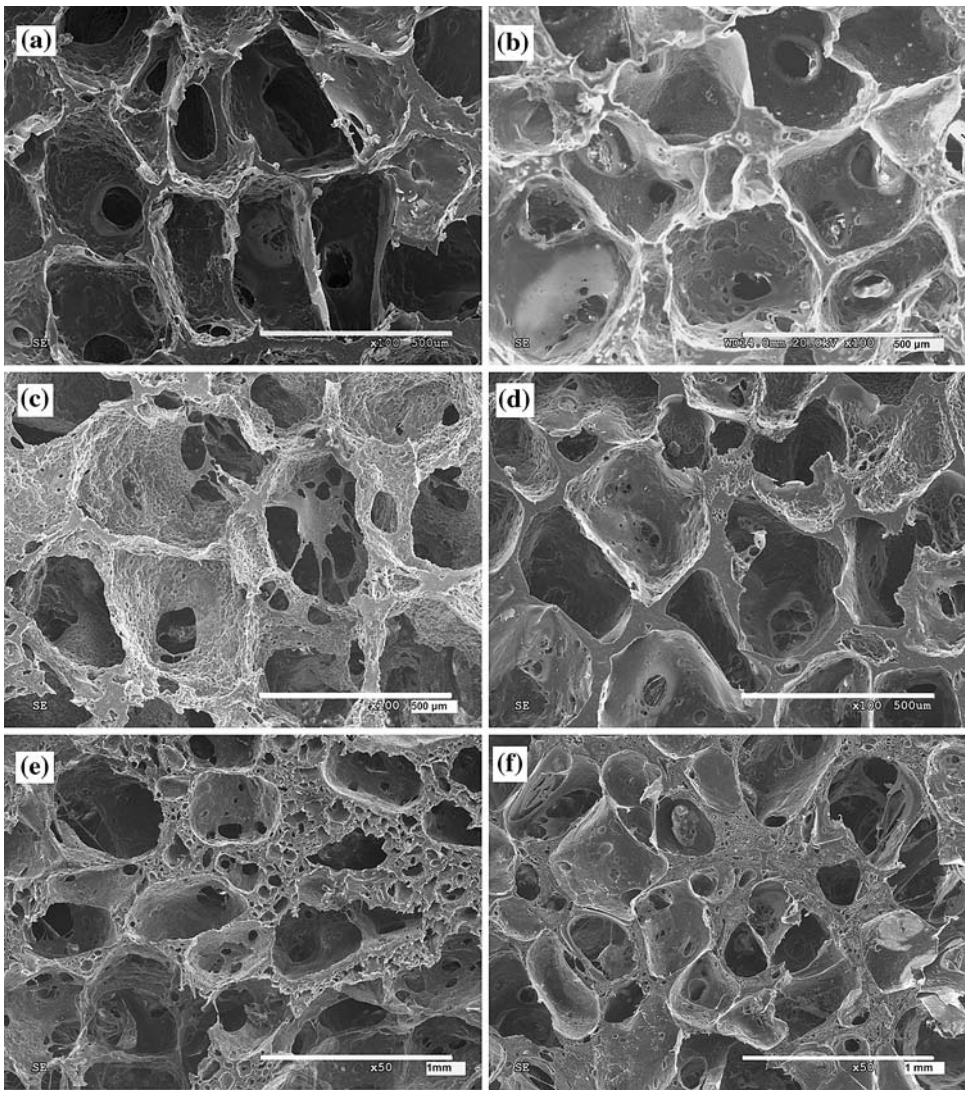

Fig. 1 SEM images of macropore structures of PUR foams prepared with NaCl particle sizes in the range of 300–420 μm and different concentrations of PUR solution: **a** PUR_50_15, **b** PUR_50_20, **c** PUR_52_15, **d** PUR_52_20, **e** PUR_70_15, **f** PUR_70_20

in these specimens. For the other types of scaffolds, the difference between total and open porosity is around 1.5% which is also an amount of closed pores (Table 2). For all scaffolds, porosity increased by a few percentages with decreasing polymer solution concentration. The highest porosity value was estimated for scaffolds based on PUR4PCL530. The cause of this trend was the increase in viscosity. When the polymer solution concentration increased, the viscosity of the solution increased to limit pore growth and favour closed pores, thereby decreasing porosity and increasing pore wall thickness. As the viscosity of the polymer solution depends on the molecular weight of the polymers (Table 1), differences in porosity for various types of polyurethane were observed [35].

The pore size distributions are shown in (Fig. 3). The PUR_52_15 scaffolds reveal multi-modal distribution of pore diameters, with two major peaks centered at 148 and 105 μm. In general, it can be noted that scaffolds prepared from 15 wt.% solution are characterized by pores with diameter above 100 μm, whereas, in scaffolds prepared from higher solution concentration, pores in the range from 44 to 90 μm are observed. Large macropores ranging in size from 300 to 420 μm, which would correspond to the size of salt particles, were not detected by this method. This arises due to mercury intrusion porosimetry restrictions. In the case of non-uniform channels, the distribution of pore volume will be affected by smaller pore throats as linkages between pores of larger diameter. Therefore, the pore size distribution given by MIP should be understood as the size distribution of the pores throats, rather than interpreted as the cavity size [36].

Analysis of SEM images of the scaffold cross-sections were performed to determine pore size distribution. The pore size distributions of the polyurethane scaffolds in terms of average Feret's diameter, are shown in (Fig. 4a–c). All scaffolds exhibit multi-modal distribution of pore diameters ranging from 2 μm to over 500 μm. According to the literature, 100 μm is assumed to be the minimum

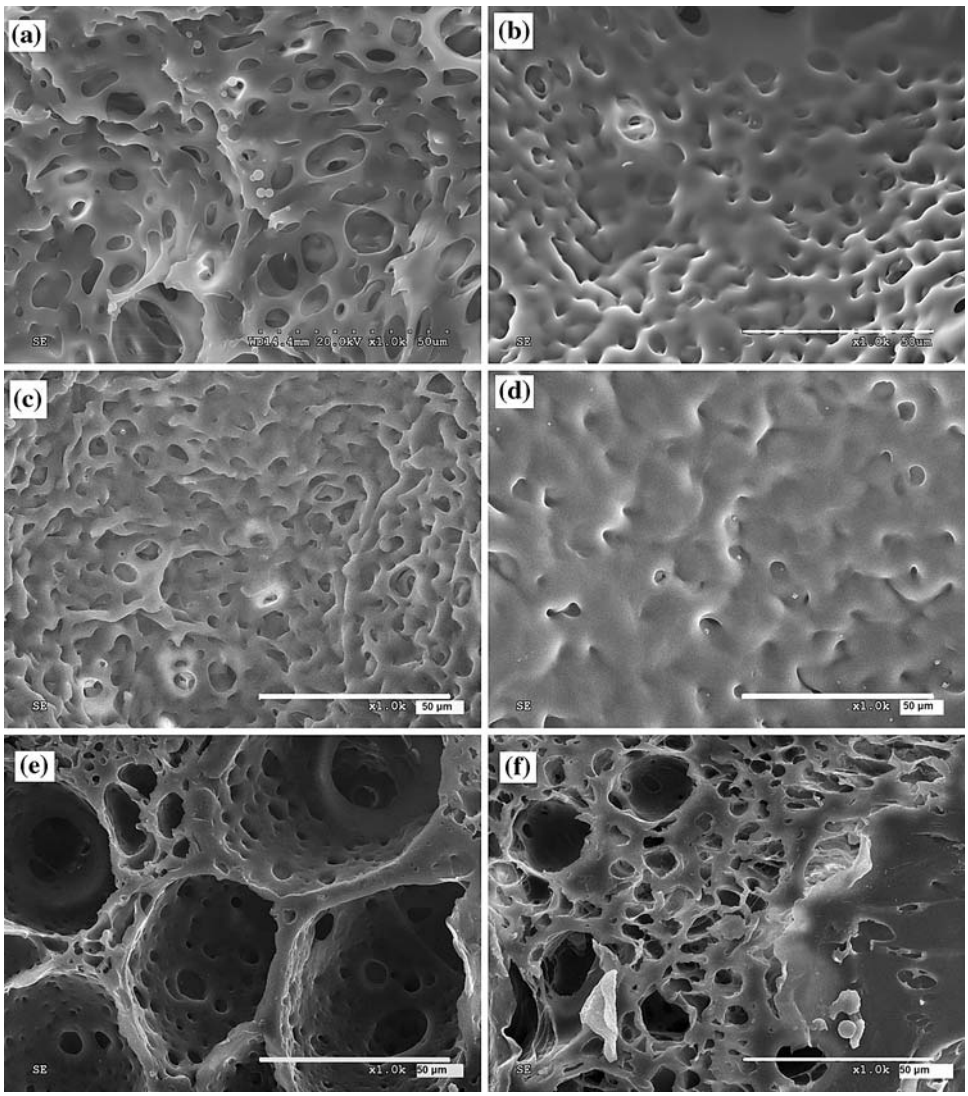

Fig. 2 SEM images of micropore structures of PUR foams prepared with NaCl particle sizes in the range of 300–420 μm and different concentrations of PUR solution: **a** PUR_50_15, **b** PUR_50_20, **c** PUR_52_15, **d** PUR_52_20, **e** PUR_70_15, **f** PUR_70_20

Table 2 Porosity data of PUR scaffolds. Open porosity (P_o) determined by mercury intrusion porosimetry and total porosity (P_t) determined gravimetrically as means ± standard deviation

Scaffold	PUR	PUR concentration (wt.%)	NaCl particles size (μm)	P_o (%) ($n = 2$)	P_t (%) ($n = 5$)
PUR_50_15	PUR4PCL1250	15	300–420	78.0 ± 0.3	78.0 ± 0.9
PUR_50_20		20		73.0 ± 2.8	73.7 ± 1.1
PUR_52_15	PUR2PCL530	15		72.4 ± 0.2	74.0 ± 1.5
PUR_52_20		20		64.7 ± 0.4	66.1 ± 1.3
PUR_70_15	PUR4PCL530	15		79.4 ± 0.1	81.9 ± 1.8
PUR_70_20		20		78.6 ± 0.1	79.4 ± 1.1

pore size conducive to bone tissue growth [6]. Thus, the micropore fraction (*Vv*%) with diameter less than 100 μm ($D < 100$ μm) and the macropore fraction with size $D > 100$ μm were calculated (Table 3). PUR_70_15 and PUR_70_20 contain 3 and 4 *Vv*% micropores respectively, while the other scaffolds only contain 1–2 *Vv*%. These data are in good agreement with SEM observations. The average Feret's diameter for macropores increases with the decreasing solution concentration and the increasing hard-segment content of the polyurethane matrix.

In order to investigate the structure–property relationships of the 3D scaffolds, the mechanical test was performed. The compressive strength of the scaffolds ranges from 0.43 to 2.38 MPa, and the compressive

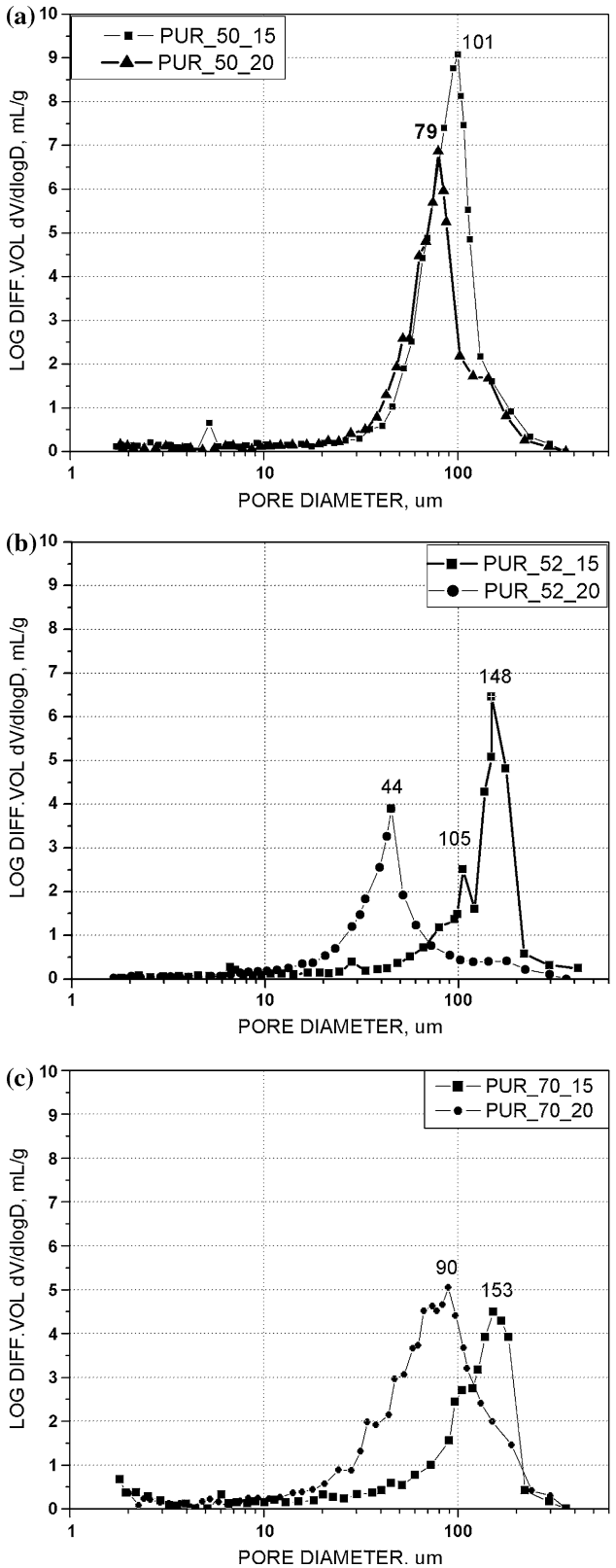

Fig. 3 Pore size distribution of the PUR scaffolds determined by mercury intrusion porosimetry (logarithmic scale for pore size) **a** PUR_50_15, PUR_50_20; **b** PUR_52_15, PUR_52_20; **c** PUR_70_15, PUR_70_20

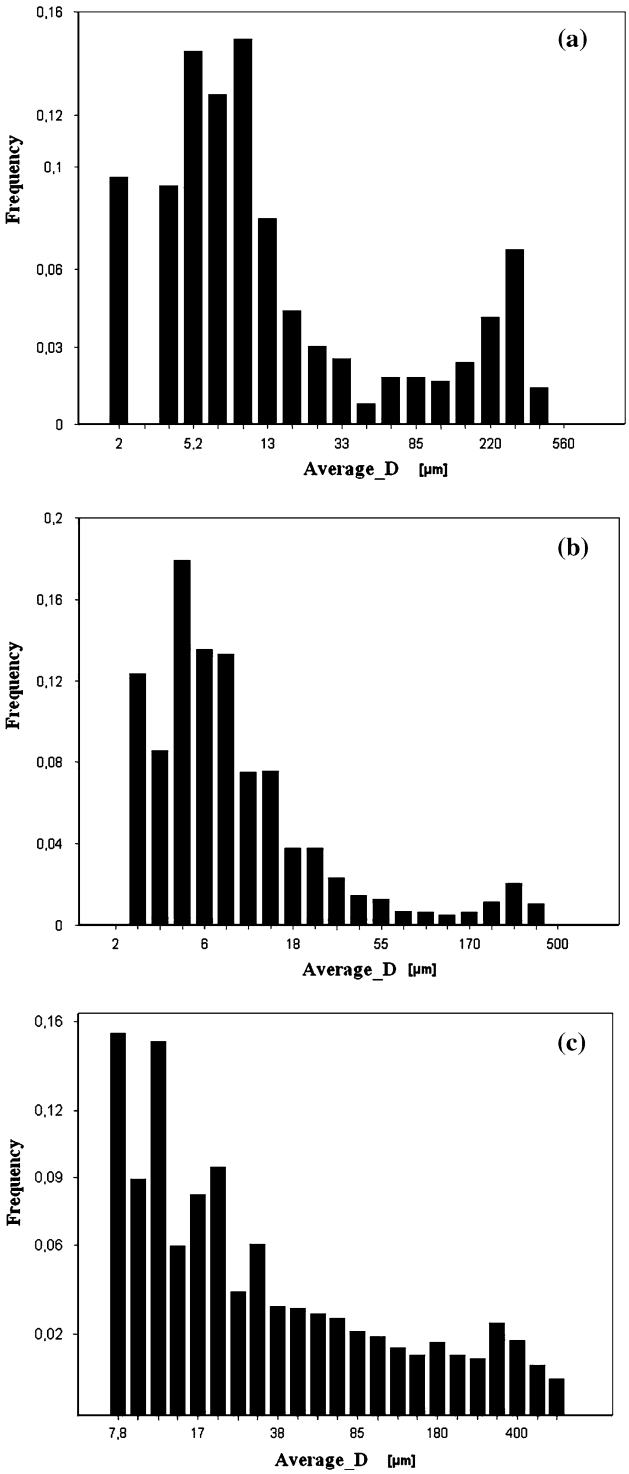

Fig. 4 Frequency distribution of average pore diameters at logarithmic scale in **a** PUR_50_15, **b** PUR_52_15, **c** PUR_70_15

modulus from 5.1 to 50 MPa (Fig. 5a, b). It can be seen that the polymer solution concentration affected the mechanical properties of the scaffolds. The PUR scaffolds made from a polymer solution concentration of 20 wt.% showed significantly higher compressive strength and

Table 3 The results of quantitative description of the structure of porous polyurethane scaffolds by analysis of SEM images

Scaffold	*Vv* (%)			Micropores	Macropores
	Total	$D < 100$ μm	$D > 100$ μm	$D < 100$ μm	$D > 100$ μm
PUR_50_15	80	2	78	15	312
PUR_50_20	70	1	69	10	302
PUR_52_15	72	2	70	11	307
PUR_52_20	66	<1	65	26	301
PUR_70_15	74	4	71	23	336
PUR_70_20	73	3	69	10	314

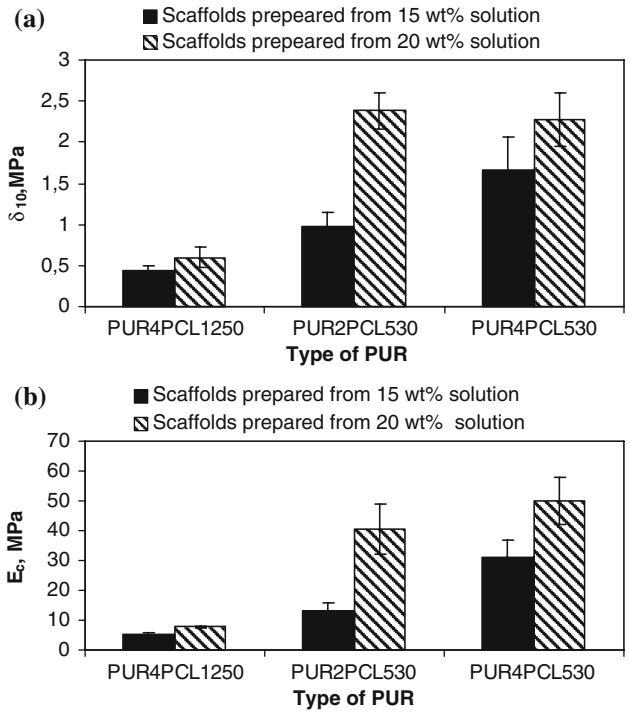

Fig. 5 Mechanical properties of PUR-based scaffolds **a** the compressive strength (δ_{10}) and **b** the compressive modulus (E_c)

compression modulus than those made from polymer concentration of 15 wt.%. The mechanical properties of the scaffold depended on the pore structure and the mass of polymer in the scaffolds. As the concentration of the polymer solution utilized increased, porosity of the scaffold decreased (Table 2) and mechanical properties increased. Also, the content of hard segment influences the mechanical properties of the obtained polyurethane scaffolds. The increase in the hard-segment content results in an increase in the intermolecular attraction which also increases the mechanical properties of the PUR. Although the porosities of PUR_50_15 and PUR_70_20 samples are nearly equal ~78%, the scaffold based on polyurethane with 70 wt.% hard segments has better mechanical properties than the scaffold with 50 wt.%.

Conclusions

In this study, we have demonstrated the possibility of processing of polyurethanes with different hard-segment contents into porous scaffolds using a salt-leaching technique combined with coagulation of polymer. The resulting scaffolds were shown to have open porosity from 64 to 80% and good interconnectivity, which makes them acceptable for applications in tissue engineering. The porosity of the scaffolds was controlled by solution concentration during polymer coagulation process.

It has been also found that the hard-segment content influences polymer coagulation process and in turn affects final architecture of the scaffolds. This varying hard-segment ratio in bulk polyurethanes can be used to control its mechanical properties. As evaluated by mechanical test, the best mechanical properties were found in scaffolds based on polyurethane with 70 wt.% hard-segment content. The further ongoing investigations aim at optimization of the processing conditions and in particular polyurethane hard-segment content.

Acknowledgements This scientific work was financially supported by the Ministry of Science and Higher Education, grant R1301901. The authors wish to thank Professor Andrzej Dworak and Dr. Barbara Trzebicka of Centre of Polymer and Carbon Materials Polish Academy of Sciences for the GPC measurements.

References

1. Palsson B, Hubbell JA, Plonsey R et al (2003) Tissue engineering. CRC Press, Boca Raton, Florida
2. Bronzino JD (2006) Tissue engineering and artificial organs. CRC Press, Boca Raton, Florida
3. Oh SH, Park IK, Kim JM et al (2007) Biomaterials 28:1664
4. Zhang Z, Wang Z, Liu S et al (2004) Biomaterials 25:177
5. Wei HJ, Liang H Ch, Lee MH et al (2005) Biomaterials 26:1905–1913
6. Whang K, Healy KE, Elenz DR et al (1999) Tissue Eng 5:35
7. Lu JX, Flautre B, Anselme K (1999) J Mater Sci Mater Med 10:111
8. Karageorgiou V, Kaplan D (2005) Biomaterials 26:5474
9. Hutmacher DW (2000) Biomaterials 21:2529

10. Zhang J, Zhang H, Wu L, Ding J (2006) J Mater Sci 41:1725. doi: 10.1007/s10853-006-2873-7
11. Draghi L, Resta S, Pirozzolo MG, Tanzi MC (2005) J Mater Sci Mater Med 16:1093
12. Chen G, Ushida T, Tateishi T (2001) Mater Sci Eng C 17:63
13. Mikos AG, Thorsen AJ, Czerwonka LA et al (1994) Polymer 35(5):1068
14. Van Tienen TG, Heijkants RGJC, Buma P et al (2002) Biomaterials 23:1731
15. Hou Q, Grijpma DW, Feijen J (2003) Biomaterials 24:1937
16. Kim SS, Park MS, Jeon O et al (2006) Biomaterials 27:1399
17. Hentze HP, Antonietti M (2002) Rev Mol Biotechnol 90:27
18. Lamba NMK, Woodhouse KA, Cooper SL (1997) Polyurethanes in biomedical applications. CRC Press, New York
19. Chen KS, Leon Yu T, Chen YS et al (2001) J Polym Res 82:99
20. Sanchez-Adsuar MS (2000) Int J Adhes Adhes 20:291
21. Ioan S, Grigorescu G (2002) Eur Polym J 38:2295
22. Tang YW, Labow RS, Santerre JP (2001) J Biomed Mater Res (2001) 56(4):516
23. Takahara A, Tashita J, Kajiyama T et al (1985) J Biomed Mater Res 19:13
24. Guan J, Fujimoto KL, Sacksa MS, Wagner WR (2005) Biomaterials 26:3961
25. Riboldi SA, Sampaolesi M, Neuenschwander P, Cossu G, Mantero S (2005) Biomaterials 26:4606
26. Grad S, Kupcsik L, Gorna K et al (2003) Biomaterials 24:5163
27. Zhang J, Doll BA, Beckman EJ et al (2003) J Biomed Mater Res 67A:389
28. Groot JH, Nijenhuis AJ, Bruin P et al (1990) Colloid Polym Sci 268:1073
29. Wojnar L, Kurzydłowski KJ, Szala J (2002) Praktyka analizy obrazu Polskie Towarzystwo Steorologiczne, Kraków
30. Ho ST, Hutmacher DW (2006) Biomaterials 27:1362
31. Hou Q, Grijpma DW, Feijen J (2003) Biomaterials 24:1937–1947
32. Heijkants RGJC, van Tienen TG, de Groot JH et al (2006) J Mater Sci 41:2423. doi:10.1007/s10853-006-7065-y
33. Lee HK, Kimb JY, Kimb YD, Shinb JY, Kimb SC (2001) Polymer 42:3893
34. Nam YS, Park TG (1999) Biomaterials 20:1783
35. Hacker M, Ringhofer M, Appel B et al (2007) Biomaterials 28:3497
36. Reignier J, Huneault MA (2006) Polymer 47:4703